Surface & Coatings Technology 203 (2009) 2357–2362

Contents lists available at ScienceDirect

Surface & Coatings Technology

journal homepage: www.elsevier.com/locate/surfcoat

Ion beam processing of sapphire single crystals

E. Alves [a,*], C. Marques [a], R.C. da Silva [a], T. Monteiro [b], C. McHargue [c]

[a] Instituto Tecnológico e Nuclear, 2686-953 Sacavém, Portugal
[b] Departamento de Física, Univ. de Aveiro, 3810-193 Aveiro, Portugal
[c] Center for Materials Processing, Univ. of Tennessee, Knoxville, USA 37996-0750

ARTICLE INFO

Available online 1 March 2009

PACS:
85.40.Ry
82.80.Yc
68.37.Lp

Keywords:
Ion implantation
Nanoparticles
α-Al_2O_3
Optical and magnetic properties

ABSTRACT

Ion implantation is a well established and widely used technique to change selectively the near surface properties of materials and particularly insulators. In this work we review the implantation of α-Al_2O_3 with different ions (transition and noble metals) to study the microscopic processes associated with the formation of the new nanostructures. The formation of nanoclusters is observed for implantation fluences above 5×10^{16} cm^{-2} of metals in sapphire at room temperature. The clustering process starts to occur during the implantation with e.g. 1–3 nm precipitates being observed in Fe-implanted samples. After annealing in a vacuum the small precipitates coalesce into larger ones following an Ostwald ripening mechanism. In the case of Fe, Co and Ti fluences above 1×10^{17} cm^{-2} create a nearly continuous distribution of metallic precipitates parallel to the c plane and surrounded by two regions containing smaller precipitates with the same orientation. The Fe and Co precipitates crystallize in phases oriented with the matrix as demonstrated by detailed multi-axial channeling and XRD analyses. Optical absorption measurements reveal a UV/blue region damage-related absorption band along with the plasmon resonance absorption band in the visible range, e.g. for gold an absorption band appears at 550 nm due to the presence of gold nanoprecipitates. The influence of annealing atmosphere on the development of the new structures will be also addressed.

1. Introduction

Metal and semiconductor nanoparticles dispersed in insulators draw much attention, envisaging applications in optoelectronic systems [1]. These nanosized particles can be introduced in dielectrics via ion implantation, sol–gel techniques, pulsed laser deposition or doping during growth [Ref. [2] and references therein]. Ion implantation has unique advantages, allowing the overcoming of thermodynamic solubility restrictions and the precise prediction of both maximum range and concentration of the implanted species in a given solid matrix. As a drawback, radiation defects are created and post implantation annealing is needed in order to eliminate these defects and to relax internal stresses induced by the presence of the implanted species and defects. However the annealing of the implantation damage has a strong influence on the final state of the implanted material.

The alpha phase of aluminum oxide (α-Al_2O_3) is one of the most studied insulator materials in which ion implantation is used to improve the mechanical properties [3] and create new optical and magnetic properties [4]. Most of these properties are due to the formation of nanosized particles embedded by the insulating host matrix. Control of the formation of such nanoparticles in α-Al_2O_3 requires the study of the interactions between the implanted species, the defects generated in the process and its annealing behavior.

In this work we present and discuss results on the implantation of metals in sapphire. The recovery of the damage and behaviour of the implanted ions will be also analyzed in detail.

2. Experimental details

Commercial sapphire (α-Al_2O_3) single crystals, 400 µm thick, with <0001> (c-samples), <11$\bar{2}$0> (a-samples) and <10$\bar{1}$0> (m-samples) orientations and optically polished surfaces were implanted at room temperature (RT) with transition and noble metal ions with energies ranging from 100 to 160 keV. The nominal fluences were in the range of 1×10^{15} to 5×10^{17} cm^{-2} and the current density was kept under 8 µA/cm^2. To recover from the implantation damage thermal annealing was carried out up to 1100 °C in air and vacuum (2×10^{-4} Pa) in a tubular furnace for 1 h. The samples went directly from RT to the temperature chosen and vice versa. RBS-C studies were performed with a 2.0 MeV He$^+$ beam after implantation and after each annealing step to characterize the structural changes. The backscattered particles were detected at 140° and close to 180° using silicon surface barrier detectors with resolutions of 13 and 18 keV respectively. The beam current was measured on target and kept below 4 nA in order to minimize the effects of charge accumulation at the surface during analysis. The optical absorption measurements were performed in the 190–1100 nm wavelength range at RT, with a Shimadzu UV3101PC

* Corresponding author. LFI, Dep. Física, Instituto Tecnológico e Nuclear, E. N. 10, 2686-953 Sacavém, Portugal. Tel.: +351 219946086; fax: +351 219941525.
E-mail address: ealves@itn.pt (E. Alves).

0257-8972/$ – see front matter © 2009 Elsevier B.V. All rights reserved.
doi:10.1016/j.surfcoat.2009.02.037

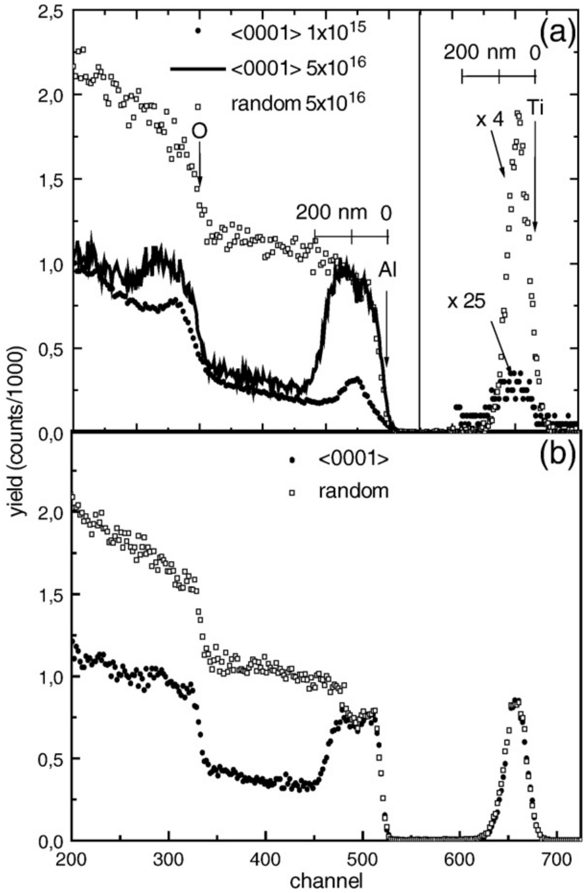

Fig. 1. Random and <0001> aligned RBS spectra showing the as-implanted behavior for a c-cut sample implanted with Ti^+ with 1×10^{15} cm^{-2} and 5×10^{16} cm^{-2} (a) and 1×10^{17} cm^{-2} (b).

double beam spectrophotometer. The XRD studies were performed using the Cu $K_{\alpha1}$ line collimated with a Gobël mirror, a 2-bounce Ge (444) monochromator and a divergent slit of 0.4×2 mm^2. The data were collected with a MBraun ASA 50M PSD detector, with a 2θ range of ≈7° acquiring for 1200 s per 2θ step. For the PL excitation in the visible spectral region we used either a Xe lamp coupled to a monochromator or the 514.5 nm line of an Ar laser. Time resolved spectra were obtained with a pulsed Xe lamp as an excitation source and a boxcar system for detection (allowing the resolution to be set up from hundreds of µs to seconds). In both cases the luminescence was dispersed by a Spex 1704 monochromator and detected by a photomultiplier. Transmission electron microscopy observations were done with a Hitachi HF-2000 field emission electron microscope operating at 200 kV.

3. Results and discussion

3.1. Structural studies

3.1.1. As implanted

The character of the ion implantation process implies the production of radiation damage, namely crystalline defects, whose amount and nature depend on several factors such as the ion beam energy and current, the implanted fluence and the characteristics of the implanted ion, the sample composition, structure and temperature and even the angle of beam incidence in the case of anisotropic materials. The dimensionality of the defects increases with the implanted fluence and hence it is possible to produce a wide range of damage, from point defects, such as vacancies and interstitials, to amorphization of entire regions, where even short range order is lost.

In the case of Ti implantation, the damage production follows a linear relation with the Ti fluence and the amorphous state is reached for a fluence of 5×10^{16} cm^{-2}. This is shown in Fig. 1(a), where the complete overlap of the random and aligned spectra in the first 120 nm in the Al lattice clearly indicates that the crystalline order necessary to steer the ion beam in to crystalline directions, a situation designated as 'channeled amorphous', is totally lost. This lower value for the amorphisation threshold with Ti, as compared with e.g. Fe (cf. Fig. 2), gives a clear indication that the chemical nature of the implanted ions plays a role in the amorphisation process [5].

In fact, in the case of iron implanted with 160 keV, the evolution of the minimum yield, measured along the channeling direction <11$\bar{2}$0> after implantation, plotted in Fig. 2, shows that even if all samples retain a large amount of damage in the entire implanted region the amorphous state is only achieved after implantation of a fluence of 5×10^{17} cm^{-2}. With such high fluences the maximum concentration reaches 3×10^{22} cm^{-3} in the implanted region and metallic conduction behavior develops.

Already at fluences of the order of 1×10^{17} cm^{-2} we start to observe the formation of metallic iron precipitates during the implantation. To illustrate this situation the TEM micrograph of Fig. 3 shows some such precipitates, with diameters of 1–3 nm. These small precipitates are surrounded by a large number of voids or empty cavities, probably evolved to keep its charge neutrality [6].

Similar results were found for high fluence implantations of Co, Ni, Cu, Hf, Ag or Au.

3.1.2. Annealing in vacuum

The post implantation annealing treatments affect both the matrix and the implanted species, depending on the temperature, atmosphere and duration of the annealing. The RBS-C spectra shown in Fig. 4 illustrate the annealing behavior of two samples implanted with 1×10^{17} cm^{-2} of Ti and Fe. The annealings were performed in vacuum for 1 h at 1000 °C. For both samples the annealing in vacuum at 800 °C produced no visible changes either in the matrix or in the as-implanted profiles.

In the case of Ti, at 1000 °C the titanium profile narrows indicating the formation of a buried Ti rich layer, Fig. 4(a). A depletion of Al from the buried layer is also observed in the random spectrum. The TEM results shown in Fig. 5 reveal the presence of large Ti precipitates at the same depth of the as implanted Ti profile. The precipitates are oriented parallel to the surface, i.e. the (0001) plane and XRD analyses reveal the presence of intermetallic Al/Ti phases. The presence of this mixed buried layer inhibits the

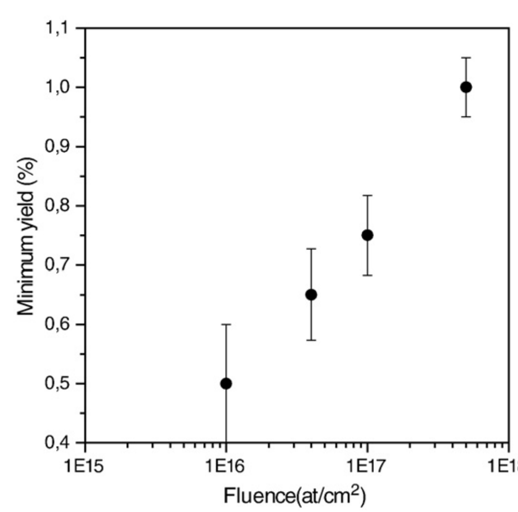

Fig. 2. Minimum normalized yield versus Fe fluence. The saturation corresponding to a channeling amorphous state is reached for 5×10^{17} cm^{-2}.